International Journal of Applied Earth Observations and Geoinformation 104 (2021) 102586

Contents lists available at ScienceDirect

International Journal of Applied Earth Observations and Geoinformation

journal homepage: www.elsevier.com/locate/jag

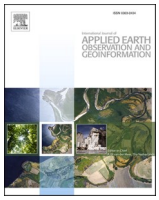

Radiance-based retrieval of total water vapor content from sentinel-3A OLCI NIR channels using ground-based GPS measurements

Jiafei Xu [a,b], Zhizhao Liu [a,b,*]

[a] Department of Land Surveying and Geo-Informatics, Hong Kong Polytechnic University, Hung Hum, Kowloon, Hong Kong
[b] Research Institute for Sustainable Urban Development (RISUD), Hong Kong Polytechnic University, Hung Hum, Kowloon, Hong Kong

ARTICLE INFO

Keywords:
GPS
Integrated water vapor (IWV)
Ocean and Land Color Instrument (OLCI)
IWV retrieval

ABSTRACT

We calibrated the integrated water vapor (IWV) data retrieved from near-infrared (NIR) channels of the Ocean and Land Color Instrument (OLCI) onboard the Sentinel-3A satellite using in-situ GPS-sensed IWV observations. Unlike conventional water vapor retrieval methodologies relying upon radiative transfer code, this method utilized a regression equation to empirically estimate GPS IWV from two NIR absorption channels at 900 nm and 940 nm. The GPS IWV data were used as reference to define the relationship between the measured radiance ratio and IWV. We collected IWV data from June 1, 2016 to May 31, 2019 from 453 GPS stations situated in the inland and coastal areas of Australia. The retrieval approach was analyzed by using different sample sizes and training datasets. The evaluation results between June 1, 2019 and May 31, 2020 in Australia indicated that the algorithm could reduce the root-mean-square error (RMSE) of the operational OLCI IWV products by 12.91% from 3.114 to 2.712 mm at the O19 channel, by 10.69% to 2.781 mm at the O20 channel, and by 11.75% to 2.748 mm for the weighted mean IWV when compared with GPS reference IWV data. When compared to European Centre for Medium-Range Weather Forecasts reference IWV data, the RMSE was reduced by 12.94% from 3.154 to 2.745 mm, by 11.04% to 2.805 mm, and by 11.93% to 2.777 mm, at the O19 channel, O20 channel, and the weighted mean, respectively. The spatiotemporal performance of the OLCI IWV measurements was improved in both station-scale and daily-scale after applying the new empirical regression retrieval method. The seasonal and land-surface-type dependence of the retrieval approach was also discussed in this research.

1. Introduction

Water vapor is one of the most dominant and most abundant natural greenhouse gases in the Earth's atmosphere (Held and Soden, 2000), which plays a vital role in affecting both weather and climate (Bojinski et al., 2014; Gao and Goetz, 1990; Held and Soden, 2000; Su et al., 2014). Since the saturation vapor pressure increases with temperature, the rise of the Earth's temperature can build up more water vapor in the troposphere (Colman, 2003; Held and Soden, 2000). This further amplifies the effect of other greenhouse gases and is responsible for air heating in the troposphere (Colman, 2003; Held and Soden, 2000). The change of atmospheric water vapor usually can lead to the change of local sudden weather phenomenon. Consequently, information on water vapor in the atmosphere is also essential for the understanding on the tropospheric diabatic heating. However, the monitoring of water vapor has challenges, because of its high variability in both space and time (Trenberth et al., 2005; Vaquero-Martínez et al., 2017). In order to develop accurate models for Earth's weather and climate prediction, it is crucial to observe the total atmospheric water vapor content as accurately as possible.

At present, most researchers mainly utilize space-based and ground-based instruments to measure the total column water vapor content in the atmosphere. The in-situ instruments used for integrated water vapor (IWV) measurements include Global Positioning System (GPS) (Davies and Watson, 1998; Gong et al., 2020), microwave radiometer (Fragkos et al., 2019), radiosonde (Gong et al., 2020), and sun-photometer (Gong et al., 2020; Holben et al., 1998). Among them, the GPS and radiosonde instruments are the most common in situ measurement techniques for water vapor observations. However, the radiosonde measurements usually have a poor spatial and temporal resolution, since the radiosonde observations are often limited to two times per day and the density of radiosonde stations is usually limited (Vaquero-Martínez et al., 2018). Instead, the GPS can provide accurate IWV observations with a high spatiotemporal resolution compared with radiosonde IWV

* Corresponding author at: Department of Land Surveying and Geo-Informatics, Hong Kong Polytechnic University, Hung Hum, Kowloon, Hong Kong.
E-mail address: lszzliu@polyu.edu.hk (Z. Liu).

https://doi.org/10.1016/j.jag.2021.102586
Received 23 July 2021; Received in revised form 10 October 2021; Accepted 11 October 2021
Available online 14 October 2021

measurements (Gong et al., 2020). Therefore, GPS IWV data have been widely employed as ground truth of water vapor to validate other satellite-based water vapor measurements (Gong et al., 2018a; Vaquero-Martínez et al., 2017, 2018; Xu and Liu, 2021).

Satellite-sensed measurements can provide continuous observation of water vapor distribution at a global scale and has been widely used in atmospheric water vapor monitoring (King et al., 2003). Over the years, numerous techniques have been developed to estimate IWV from space-sensed measurements utilizing different electromagnetic spectra: visible (VIS) (Lang et al., 2003; Wang et al., 2014), near-infrared (NIR) (Abbasi et al., 2020; Gao and Kaufman, 2003; Gong et al., 2018b; Kaufman and Gao, 1992), infrared (IR) (Seemann et al., 2003), and microwave (MW) (Liu et al., 2020; Turner et al., 2007). Wang et al. (2014) developed a two-step operational Ozone Monitoring Instrument (OMI) water vapor retrieval approach using the 430–480 nm spectral region, and the water vapor estimation results generally showed a good agreement with those retrieved from the Moderate Resolution Imaging Spectroradiometer (MODIS) instrument and the Aerosol Robotic NETwork (AERONET) sun photometer instrument, with the R^2 of 0.93 to 0.97 and 0.49 to 0.75, respectively. Gao and Kaufman (2003) utilized MODIS NIR bands (channels 2, 5, 17, 18, and 19) to derive IWV over land using 2-channel and 3-channel ratio methods. The typical error in estimated water vapor values is 5% ~ 10%, when compared with reference ground-based microwave radiometers measurements. The nighttime MODIS water vapor products, i.e., MOD07 or MYD07, are generated using IR spectral bands (Seemann et al., 2003). The total column water vapor retrieval results over the Iberian Peninsula showed a comparable relationship with observations from in-situ radiosonde sites, with a standard deviation of 0.5 cm (Sobrino et al., 2015). Liu et al. (2020) proposed a physical retrieval method to compute the total column water vapor content over land through the use of passive microwave bands at 165.50 GHz and 183.31 GHz. By comparison with GPS retrieved IWV data, the coefficient of determination (R^2), root-mean-square error (RMSE), and bias of the retrieved water vapor estimates were 0.90, 0.43, and − 0.02 cm, respectively. These algorithms mainly used differential absorption methodology (Schläpfer et al., 1998) with an atmospheric radiative transfer equation (Gao and Kaufman, 2003; Liu et al., 2020; Seemann et al., 2003; Wang et al., 2014).

European Space Agency (ESA) has developed numerous satellite observations used for the operational needs of the Copernicus program, named Sentinel series (http://www.esa.int/Applications/Observing_the_Earth/Copernicus/Overview4). Each Sentinel mission relies upon a constellation of two satellites to provide robust datasets for Copernicus services. The Sentinel-3 family, a multi-instrument mission, is designed to provide observations for ocean forecasting, environmental monitoring, and climate studies (Donlon et al., 2012). Sentinel-3A and 3B were launched on 16 February 2016 and 25 April 2018, respectively. The system of these two satellites makes it possible to gain an image of the Earth's surface within a day (Lamquin et al., 2020). An Ocean and Land Color Instrument (OLCI), based on the proven heritage of the Medium Resolution Imaging Spectrometer (MERIS) sensor on-board the ENVISAT satellite platform, is on board both Sentinel-3A and Sentinel-3B satellite platforms (Donlon et al., 2012; Lamquin et al., 2020). Their main difference is that MERIS has 15 spectral bands whereas OLCI has 21 channels, and the OLCI instrument can provide a spatial resolution of 300 m over all surfaces (Lamquin et al., 2020).

Operational approach has been developed to retrieve IWV estimates using Sentinel-3 OLCI measurements, which is to relate the IWV content to the radiance ratio of OLCI bands O18 and O19 (equivalent to MERIS bands M14 and M15) centered at 885 nm and 900 nm, respectively (Fischer et al., 2010a). The water vapor retrieval is performed utilizing a neural network as well as an atmospheric radiative transfer model Matrix Operator Model (MOMO) (Fischer et al., 2010a). MERIS-sensed IWV has showed a good agreement with in-situ microwave radiometer and GPS measurements in Oklahoma, with an RMSE value of 1.64 mm and 1.22 mm, respectively (Fischer et al., 2010b). The OLCI-derived IWV and ground-based GPS-sensed IWV observations have shown a bias of −0.57 ± 2.90 mm for Sentinel-3A and 2.42 ± 3.41 mm for Sentinel-3B over Greece (Mertikas et al., 2020).

The current OLCI IWV data are only retrieved from absorption channel O19 at 900 nm using the O18 channel at 885 nm as the window channel. The data of another NIR channel O20 at 940 nm have not been used yet. However, another absorption channel O20 (940 nm) has not been investigated though it is strongly recommended (Fischer et al., 2010a). It is expected that the addition of the new absorption channel will benefit IWV derivation. Actually, the water vapor absorption band located at 940 nm has been utilized for atmospheric water vapor observations in sensors of other satellite missions such as MODIS and MERIS (Abbasi et al., 2020; Gao and Kaufman, 2003; Kaufman and Gao, 1992).

In this paper, we utilized both absorption channels O19 and O20 to retrieve IWV data. This is the first time in the research community to use both O19 and O20 channels to estimate water vapor from Sentinel-3A OLCI. We developed a model in this study for the Sentinel-3A OLCI sensor to retrieve atmospheric column water vapor from OLCI radiance data, where ground-based GPS IWV data were used to empirically establish the relationship between the IWV and the radiance ratio of water vapor absorption channels. The Sentinel-3A OLCI measurements were employed in this research because it has a longer observation time period and has accumulated much more raw data than the Sentinel-3B. In contrast to the traditional IWV retrieval approaches that rely on atmospheric radiative transfer codes, the model in this study employs an empirical regression function to calculate OLCI-sensed IWV estimations from two NIR water vapor absorption bands O19 (900 nm) and O20 (940 nm).

The paper has been organized in the following structure. Section 2 provides a detailed description of the data sets used for model construction and verification in this study. The water vapor retrieval model using GPS and OLCI measurements is presented in Section 3. In Section 4, the retrieval results and corresponding analysis/validation are described. The independent validation results for different seasons and land surface covers are also discussed in Section 4. Section 5 summarizes the main findings in this work.

2. Data and pre-processing

The research area covers the inland and coastal regions of Australia, with latitude between 10°41′S and 43°39′S and longitude between 112°57′ E and 153°45′ E (see Fig. 1). We utilized three types of data sets in our study: GPS IWV data, Level-1 and -2 OLCI data, and the European Centre for Medium-Range Weather Forecasts (ECMWF) IWV data (see Table 1). As displayed in Fig. 1, 453 in-situ GPS stations were selected to

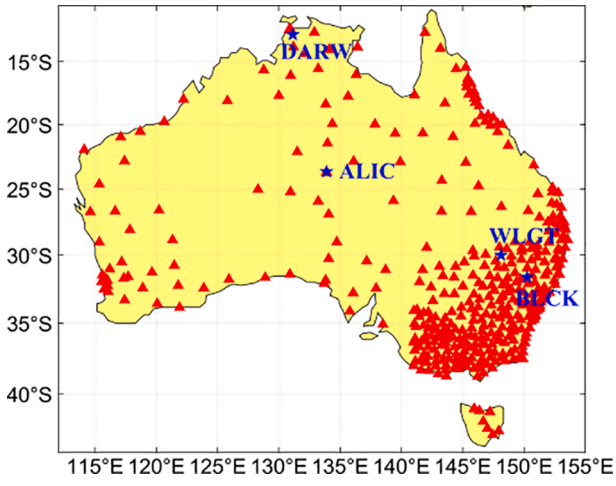

Fig. 1. The spatial locations of 453 ground-based GPS sites across Australia.

Table 1
Summary of data used for algorithm construction and evaluation.

Data source	Time span	Temporal resolution	Spatial resolution	Data description	Function
GPS observations	June 1, 2016–May 31, 2019	hourly	453 stations, point data	meteorology data	model development
OLCI Level-1 products	June 1, 2016–May 31, 2019	4-day	300 m	Top-Of-Atmosphere (TOA) radiances	model development
GPS observations	June 1, 2019–May 31, 2020	hourly	453 stations, point data	meteorology data	model verification
OLCI Level-1 products	June 1, 2019–May 31, 2020	4-day	300 m	Top-Of-Atmosphere (TOA) radiances	model verification
OLCI Level-2 products	June 1, 2019–May 31, 2020	4-day	300 m	IWV columns	model verification
ECMWF reanalysis products	June 1, 2019–May 31, 2020	hourly	0.25° × 0.25°	column water vapor	model verification

develop and evaluate our empirical water vapor retrieval model. The land surface types over these ground-based sites vary widely from arid to dark vegetation areas.

2.1. GPS data

The ground-based water vapor data, employed to build and validate the new model, were derived from the Geoscience Australia tropospheric zenith path delay (ZPD) products (Pigram, 2012). We converted the ZPD products into the ground-based IWV estimation data, which has a temporal resolution of one hour. More details of this conversion process are described in Section 3. GPS derived IWV data between June 1, 2016 and May 31, 2020 from 453 GPS stations over Australia (see Fig. 1) were used to construct and assess the new approach: the GPS-sensed IWV observations from June 1, 2016 to May 31, 2019 were used for model development, and the IWV from June 1, 2019 to May 31, 2020 were used for algorithm evaluation (see Table 1). As GPS IWV estimates may not exactly synchronize with the OLCI over-pass time, we allowed the two data sources to have a time difference of 30 min between each other. This relies on the assumption that the water vapor in the atmosphere varies slowly and smoothly other than rainfall or other events occurring in the very short time interval of GPS- and OLCI-sensed observations, i.e., less than 30 min.

2.2. Sentinel-3A OLCI data

The OLCI sensor, an imaging spectrometer evolving from the ENVISAT MERIS instrument, has provided three levels of data products for the general public (Fletcher, 2010). All the Sentinel-3A OLCI data, i.e., Level-1 OLCI radiance data and Level-2 OLCI IWV data, were collected from the ESA Copernicus Open Access Hub. The OLCI L2 IWV product is generated using the water vapor absorption channel at 900 nm (O19) only, with a spatial resolution of 300 m (Fischer et al., 2010a). The neural network as well as the atmospheric radiative transfer model MOMO was used in the official OLCI IWV retrieval algorithm (Fischer et al., 2010a). The Level-1 OLCI products for the period June 1, 2016 to May 31, 2019 were utilized to develop water vapor retrieval model. The OLCI data from June 1, 2019 to May 31, 2020 were employed to verify the performance of the developed model. A total of 2063 OLCI images distributed over the GPS stations were used to train the water vapor retrieval method, and more than 1000 scenes including Level-1 and Level-2 products were selected as validation datasets. For each OLCI imagery, the satellite pixels closest to each GPS station were used for model development and validation. Three NIR channels of the OLCI instrument, including two absorption channels O19 and O20 and one window channel O18, were utilized in our study, and the detailed description is given in Table 2.

Satellite-based water vapor measurements usually have a poor accuracy under cloudy conditions because the NIR wavelengths of the satellite-based instruments cannot penetrate clouds, especially thick clouds (He and Liu, 2019). Thus, the Level-1 OLCI product file qualityFlags was utilized as a quality control in our research to obtain confident clear land pixels for algorithm development and evaluation. Namely, only OLCI pixels flagged as "LAND" (land surface and clear sky) have been taken into account in this paper. The OLCI pixels closest to in-situ GPS stations were utilized in our study, and their spatial distance was required to be smaller than 10 km.

Table 2
Band characteristics of the sentinel-3A OLCI sensor.

Band number	O18	O19	O20
Center (nm)	885	900	940
Width (nm)	10	10	20
Lmin (W/(m^2·sr·μm))	2.80	2.05	0.94
Lref (W/(m^2·sr·μm))	6.00	4.73	2.39
Lsat (W/(m^2·sr·μm))	281.0	237.6	171.7
SNR@Lref	395	308	203
Spatial resolution (m)	300	300	300
Description	window channel	absorption channel	absorption channel

2.3. ECMWF data

The ECMWF atmospheric reanalysis products, i.e., the newest generation of ECMWF Reanalysis (ERA5) (Hersbach et al., 2020; Hoffmann et al., 2019), were also used in this study to quantitatively assess the accuracy of OLCI-derived IWV data. ERA5 total column water vapor products, available in the Climate Data Store (CDS), have a high-temporal resolution of one hour as well as a high-spatial resolution of 0.25° × 0.25° (see Table 1) (Hersbach et al., 2020). This hourly output resolution can provide a more detailed description of the evolution of particular weather events. Compared with ground-based GPS IWV observations, the ERA5 IWV data have an RMSE value of 1.84 mm (Wang et al., 2020), smaller than other reanalysis products, such as the Japanese 55-year Reanalysis (JRA-55) (Ebita et al., 2011) and the National Centers for Environmental Prediction/National Center for Atmospheric Research (NCEP/NCAR) (Kalnay et al., 1996). In recent work conducted by Yu et al. (2021), the global standard deviations between ERA5 PWV and GPS PWV were reported to be usually lower than 0.3 cm. In this paper, ERA5 reanalysis data during the period from June 1, 2019 to May 31, 2020 were selected as the second validation dataset (see Table 1) to evaluate the newly developed water vapor retrieval model. The ERA5 data were obtained according to the locations of the 453 GPS stations located in the inland and coastal areas of Australia, where the ERA5 pixels closest to in-situ GPS stations were selected. The spatial distance between them was required to be less than 50 km.

3. Methods

3.1. Ground-based GPS water vapor retrieval

When GPS signals pass through the troposphere, the signals are delayed. This delay can be converted from the signal's slant direction to the zenith direction using the mapping functions (Bevis et al., 1992; Ning et al., 2016). In the zenith direction, it is called zenith tropospheric delay (ZTD). The *ZTD* can be classified into two different components: the zenith hydrostatic delay (ZHD) and the zenith wet delay (ZWD) (Bevis et al., 1992).

$$ZTD = ZHD + ZWD \quad (1)$$

By using ancillary data, i.e., surface temperature and atmospheric pressure, which were acquired from ECMWF reanalysis products, the ZHD can be precisely modeled using empirical models (Chen and Liu, 2015). It can be calculated as below (Bevis et al., 1992):

$$ZHD = \frac{(2.2997 \pm 0.0024)P_s}{1 - 0.00266cos2\varphi - 0.00028H} \quad (2)$$

where P_s is the atmospheric pressure at the GPS station; φ is the latitude of the GPS station; and H is the height of the GPS station.

The remaining part ZWD can be estimated from GPS observations, which has been routinely conducted in the GPS community (Bevis et al., 1992). The spatiotemporal variation of ZWD is more important, in comparison with the ZHD which changes slowly in both space and time. The contribution of ZWD is mainly caused by the water vapor in the atmosphere and it can be used to estimate the IWV. The relationship between water vapor and ZWD is given below (Bevis et al., 1992):

$$W_G = \Pi \cdot \mathrm{ZWD} \quad (3)$$

where the W_G is the IWV derived from the ground-based GPS observations, and Π is a constant related to the weighted mean temperature of the atmosphere, which can be estimated from the temperature in the land surface (Wang et al., 2016).

In this work, the ERA5 ancillary data, including surface temperature and atmospheric pressure, were employed to model *ZHD*, as well as to compute the coefficient Π. Once the *ZHD* and Π are obtained, GPS-retrieved IWV data can be estimated from Geoscience Australia GPS tropospheric ZTD products. Water vapor data selected from 453 GPS stations over Australia were used to construct the algorithm and validate the OLCI-sensed IWV data.

3.2. Space-based water vapor retrieval using OLCI radiance data

The instruments on board Earth observation satellites can provide data of high spatial resolution for atmospheric water vapor retrieval. Currently, the OLCI sensor mainly uses two spectral channels O18 and O19 to retrieve operational Level-2 IWV products using a differential absorption approach (Fischer et al., 2010a). The two bands are close to each other. O19 at 900 nm is the absorption channel and the O18 at 885 nm is a non-absorption (window) (Fischer et al., 2010a). The neural network as well as atmospheric radiative transfer model MOMO were employed in the IWV retrieval (Fischer et al., 2010a). The retrieval algorithm can be calculated as (Bennartz and Fischer, 2001):

$$W = a_0 + a_1 log(M) + a_2 log^2(M) \quad (4)$$

$$M = \frac{O_{19}}{O_{18}} \quad (5)$$

where W is the derived IWV estimation, and a_0, a_1, and a_2 are equation coefficients, and M is the ratio of the radiance measured in OLCI channel O19 to that of O18.

As suggested in the previous research, there is a systematic overestimation in the MERIS or OLCI water vapor products when compared with in-situ GPS observations (Fischer et al., 2010b; Mertikas et al., 2020). In addition, the work conducted by Bennartz and Fischer. (2001) showed that the variable observation geometries have only little effect on the performance of the MERIS IWV estimation, except for very high latitudes. The OLCI instrument is evolved from the MERIS instrument, and they have the same official water vapor retrieval algorithms (Bennartz and Fischer, 2001; Fischer et al., 2010a). Neither MERIS nor OLCI official IWV retrieval method uses a mapping function for the observations from slant direction, as the satellite-based MERIS and OLCI IWV retrievals are barely affected by the variable observation geometry. This is different from other satellite-based instruments such as the MODIS and MERSI sensors where a mapping function is used in IWV retrieval algorithm of both MODIS and MERSI. The satellite-based MODIS and MERSI IWV retrievals are greatly affected by the variable observation geometry (Gao and Kaufman, 2003).

The crucial step to improve the accuracy of IWV estimation is to find a way to more accurately describe the relationship between the ratio of the radiance and the IWV content. In this study, the empirical regression analysis was mathematically performed to re-construct their relationship (the measured radiance ratio versus the total atmospheric water vapor content), where ground-based GPS derived IWV are considered as the truth water vapor observations. Our algorithm does not use mapping function as well, which is the same as the official OLCI IWV retrieval approach. To show the validity of doing this, a test of using and without using mapping function is conducted and the result is shown below in Fig. 2.

In Fig. 2, we showed the result of a three-month dataset from June 1, 2019 to August 31, 2019 with and without using a mapping function. The mapping function for OLCI IWV retrievals is same as that for MODIS IWV retrievals (Gao and Kaufman, 2003). The results in Fig. 2(a), Fig. 2(c), and Fig. 2(e) are obtained without using mapping function in OLCI IWV retrieval. The results in Fig. 2(b), Fig. 2(d), and Fig. 2(f) are obtained using a mapping function. It can be seen that the difference between the two sets of result is negligibly small. The results are consistent with those shown in the previous work by Bennartz and Fischer (2001). Based on our test result, we decide to follow the official OLCI IWV retrieval approach, not using mapping function in IWV retrieval.

3.3. New water vapor retrieval model

Different from the current method where only the absorption channel O19 is used, we used both absorption channels O19 and O20 in our method to study the relationship between GPS IWV and the radiances at the two channels. To eliminate the effect of cloudy condition on the IWV retrieval, only non-cloudy land pixels are selected for regression analysis in this work.

As shown in Fig. 3, a total of 60,301 pixels (300 m resolution) in each Sentinel-3A OLCI channel O19 (900 nm) and O20 (940 nm) were selected to analyze the empirical relationship between GPS IWV and the measured radiance ratio. Evidently, an exponential function can be used to characterize this relationship. After experimentally testing different functions, the fitting function between the GPS-derived IWV and the radiance ratio is identified as:

$$OR_i = aexp\left(bW_i^*\right) + cexp(dW_i^*) \quad (6)$$

$$OR_i = \frac{O_i}{O_{18}} \quad (7)$$

where W_i* is retrieved IWV estimates, and a, b, c, and d are the regression parameters to be calculated, and OR_i is the measured radiance ratio, and the subscript i represents the absorption channel O19 or O20.

IWV values can be derived from each individual OLCI absorption band. As water vapor in the atmosphere has significantly different absorption characteristics at the OLCI band bandpasses, the two channels O19 and O20 have different water vapor sensitivities under the same atmospheric condition (Kaufman and Gao, 1992). For example, the water vapor absorption band centered at 940 nm is more sensitive to dry conditions, whereas the water vapor absorption band located at 900 nm is more sensitive to wet conditions (Kaufman and Gao, 1992). Thus, the water vapor values estimated from the O19 and O20 bands can be different even under the same atmospheric condition. Accordingly, the weighted mean water vapor value computed from the two absorption bands has a wider suitability under various atmospheric conditions. It is defined as:

$$W_m^* = f_1 W_{19}^* + f_2 W_{20}^* \quad (8)$$

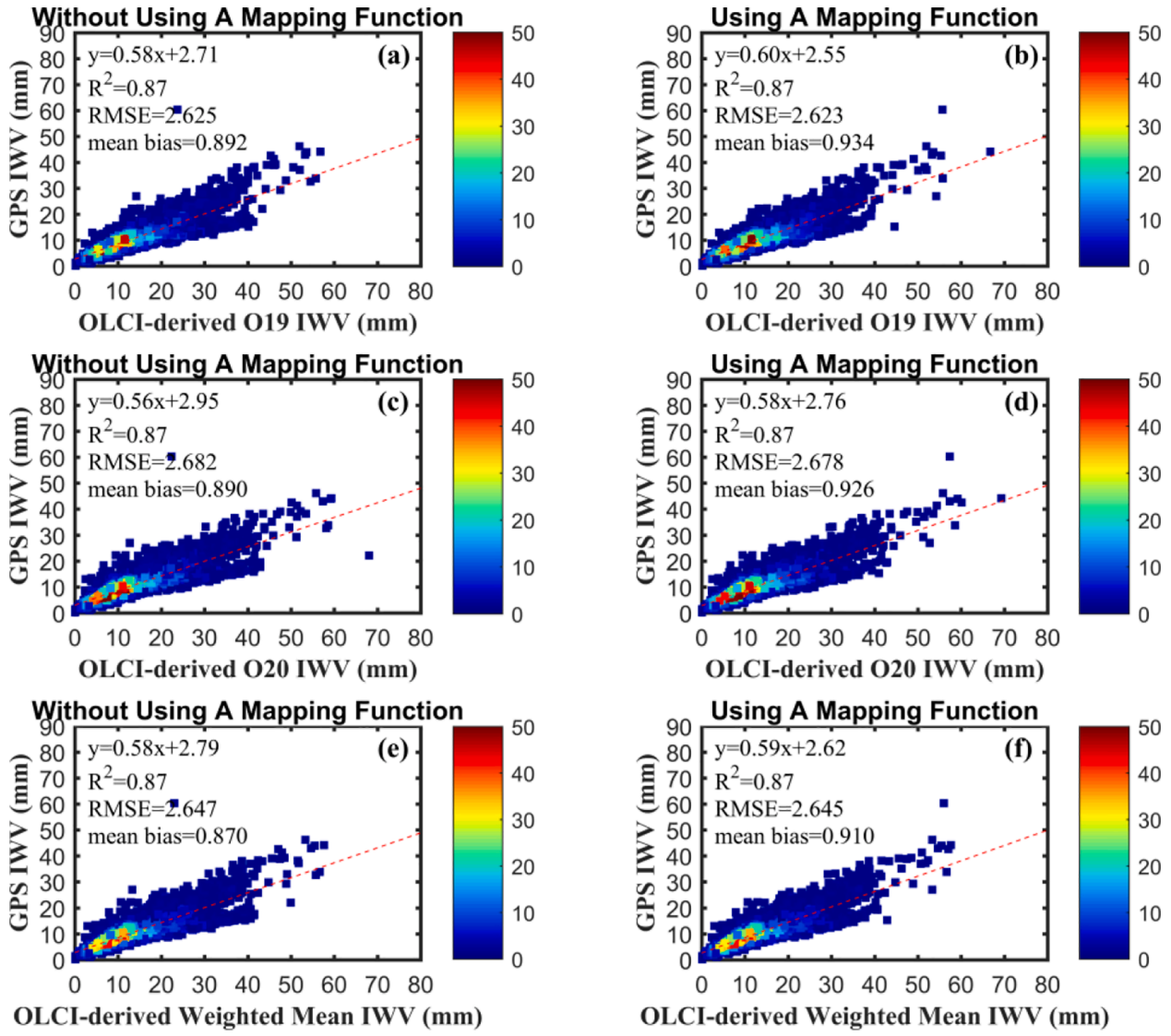

Fig. 2. Comparison of OLCI IWV retrieval results against reference GPS IWV retrieval results using data from June 1, 2019 to August 31, 2019 in Australia. (a), (c), and (e): results are obtained without using a mapping function in OLCI IWV retrieval. (b), (d), and (f): results are obtained using a mapping function in OLCI IWV retrieval.

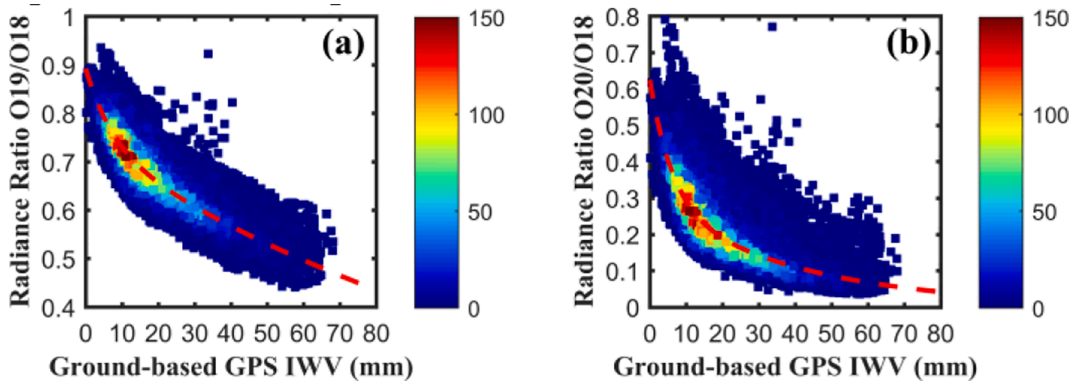

Fig. 3. Scatter points for the total amount of atmospheric water vapor measured from GPS observations with respect to the measured radiance ratio of two water vapor absorption channels of OLCI, (a) radiance ratio of O19 band to O18 band; (b) radiance ratio of O20 band to O18 band. The dashed red lines show empirical regression fitting. The color bar indicates the frequency of the water vapor values (red highest frequent and blue lowest frequent). (For interpretation of the references to color in this figure legend, the reader is referred to the web version of this article.)

where W_{19}* and W_{20}* are water vapor values estimated from the O19 and O20 bands, respectively; and f_1 and$f_2$are the weighting functions. They were computed as the normalized values of the sensitivity in each spectral band:

$$f_i = \frac{\eta_i}{\eta_1 + \eta_2} \tag{9}$$

where η_i is the slope of the graph between the measured radiance ratio and the IWV content for each OLCI water vapor absorption band. It is calculated to represent the sensitivity in each absorption channel:

$$\eta_i = \left| \frac{dOR_i}{dW_i^*} \right| \tag{10}$$

4. Results

4.1. Algorithm analysis using different sample sizes

A total of 60,301 collocations of OLCI-GPS matched IWV data points were selected for model development. Usually, the empirical regression approach depends highly on the training dataset. As a result, different training data can generate different outcomes. To study the reliability of the newly developed water vapor retrieval algorithm, we employed several tests through different sample sizes in this research. As presented in Table 3, the statistical parameters, root-mean-squares-error (RMSE) and standard deviation (SD) vary slightly with different sample sizes, indicating that this empirical regression model is reliable for different sample sizes. For instance, at the water vapor absorption channel O19, the RMSE values for the different sample sizes against the ground-based GPS-derived IWV are 2.793, 2.856, 2.872, and 2.781 mm, and the standard deviations of radiance ratio are 0.098, 0.094, 0.085, and 0.082, respectively. For the other absorption band O20, the RMSE values are in the range of 2.945 to 3.084 mm, with the standard deviations of radiance ratio ranging from 0.140 to 0.151. Additionally, the mean bias, calculated by subtracting reference GPS IWV data from the OLCI IWV observations, showed overall positive values (overestimated). Furthermore, we randomly classified the training dataset into five independent training and testing subsets. The regression parameters for each atmospheric water vapor absorption channel were listed in Table 4. Results showed that regression coefficients of different datasets were very consistent, and they varied only slightly for different independent testing subsets.

4.2. Evaluation of new OLCI water vapor retrieval model

To further validate the accuracy of this novel OLCI water vapor retrieval model, we conducted an evaluation of OLCI-sensed IWV versus GPS observations collected from June 1, 2019 to May 31, 2020 over Australia. A total of 22,082 collocations under clear conditions were obtained from 453 GPS sites. These stations are located in the inland and coastal areas of Australia, covering different climate zones and land surface covers. In addition, the ERA5 IWV data were also used as reference water vapor values to verify the new OLCI IWV data.

Evaluation results shown in Fig. 4 suggest that the new OLCI IWV data perform better than the official OLCI L2 IWV products, with overall higher correlations and smaller RMSE against both GPS IWV and ERA5 IWV reference data. It should be noted that the operational OLCI IWV products were retrieved using a neural network with an absorption channel O19 centered at 900 nm and a non-absorption channel O18 centered at 885 nm (Fischer et al., 2010a). For the IWV estimated from OLCI O19 channel, the RMSE has reduced 12.91% from 3.114 mm to 2.712 mm compared with GPS-derived IWV, and it has reduced 12.94% from 3.153 mm to 2.745 mm when compared with ERA5 reanalysis products. For OLCI O20 IWV data, the RMSE has reduced 10.69% to 2.781 mm and 11.04% to 2.805 mm when compared to the reference GPS and ECMWF data, respectively. For the weighed mean IWV estimated from both OLCI O19 and O20 bands, the RMSE has reduced 11.75% from 3.114 mm to 2.748 mm against GPS IWV and has reduced 11.93% to 2.777 mm when compared with ERA5 IWV. Results indicated that the OLCI O19 IWV estimation in this work showed the best agreement with GPS and ERA5 IWV datasets, when compared with OLCI O20 IWV and weighted mean IWV. It should be noted that OLCI did not produce IWV products on channel O20. For the convenience of comparison with our new IWV at O20 channel, in this study we considered the IWV products from channel O20 same as those from O19.

It is noted that the new OLCI O19 IWV estimates performed better than the new OLCI O20 IWV estimates as well as the new OLCI weighted mean IWV estimates. The most possible reason is that the climate in Australia is generally humid especially in the southeast Australia region. As the O19 channel at 900 nm has high sensitivity under wet conditions (Kaufman and Gao, 1992), it may show better performance in OLCI IWV retrieval in Australia in a humid climate.

4.3. Seasonal analysis

The dependence of water vapor retrieval performance on different seasons were analyzed and discussed. This is because different seasons are associated closely with the annual cycle of water vapor in the atmosphere (Vaquero-Martínez et al., 2017). We divided the validation period from June 1, 2019 and May 31, 2020 into four seasons, namely, spring (July 2019 to September 2019), summer (October 2019 to December 2019), autumn (January 2020 to March 2020), and winter (Jun 2019, and April 2020 to May 2020). Seasonal validation results are shown in Figs. 5 and 6. The new OLCI IWV had smaller RMSE values in each season. The new IWV results were more accurate than the Level-2 OLCI IWV products, when compared to the reference GPS-derived and ERA5 IWV data. For instance, in spring, the RMSE has reduced 12.94% from 3.145 mm to 2.738 mm for OLCI-derived IWV data from O19 channel, 11.03% to 2.798 mm for OLCI-derived IWV data from O20 channel, and 12.21% to 2.761 mm for weighted mean OLCI-derived IWV data from both O19 and O20 channels, when compared to reference in-situ GPS-derived IWV data.

When compared to reference ERA5 IWV data, it has reduced 13.28% from 3.147 mm to 2.729 mm, 10.71% to 2.810 mm, and 12.07% to 2.767 mm, for the OLCI-derived IWV data from O19 channel, O20 channel, and both two channels, respectively. The RMSE values and reductions for OLCI-retrieved IWV data in each season are shown in Table 5. It is clearly observed that new OLCI-derived IWV estimation

Table 3
The results obtained from using different sample sizes for water vapor retrieval algorithm development. The mean difference and RMSE of each training dataset versus GPS measurements, and the Standard Deviation (SD) of radiance ratio in each test of different numbers of samples, are calculated for water vapor absorption bands O19 and O20.

Training data (%)	Number of points	O19			O20		
		mean bias (mm)	RMSE (mm)	SD of radiance ratio	mean bias (mm)	RMSE (mm)	SD of radiance ratio
90%	54,271	0.253	2.793	0.098	0.548	2.972	0.151
70%	42,211	0.239	2.856	0.094	0.531	3.035	0.147
40%	24,120	0.066	2.872	0.085	0.374	3.084	0.143
10%	6,030	−0.134	2.781	0.082	0.183	2.945	0.140

Table 4
Summary of regression coefficients for five independent training subsets over Australia using GPS IWV data from June 1, 2016 to May 31, 2019.

Training dataset	O19				O20			
	a	b	c	d	a	b	c	d
1	0.156	−1.349	0.738	−0.066	0.339	−1.615	0.287	−0.240
2	0.159	−1.301	0.733	−0.064	0.345	−1.760	0.298	−0.251
3	0.153	−1.352	0.738	−0.066	0.339	−1.596	0.283	−0.233
4	0.154	−1.196	0.730	−0.064	0.325	−1.505	0.280	−0.236
5	0.159	−1.435	0.741	−0.068	0.342	−1.717	0.297	−0.253

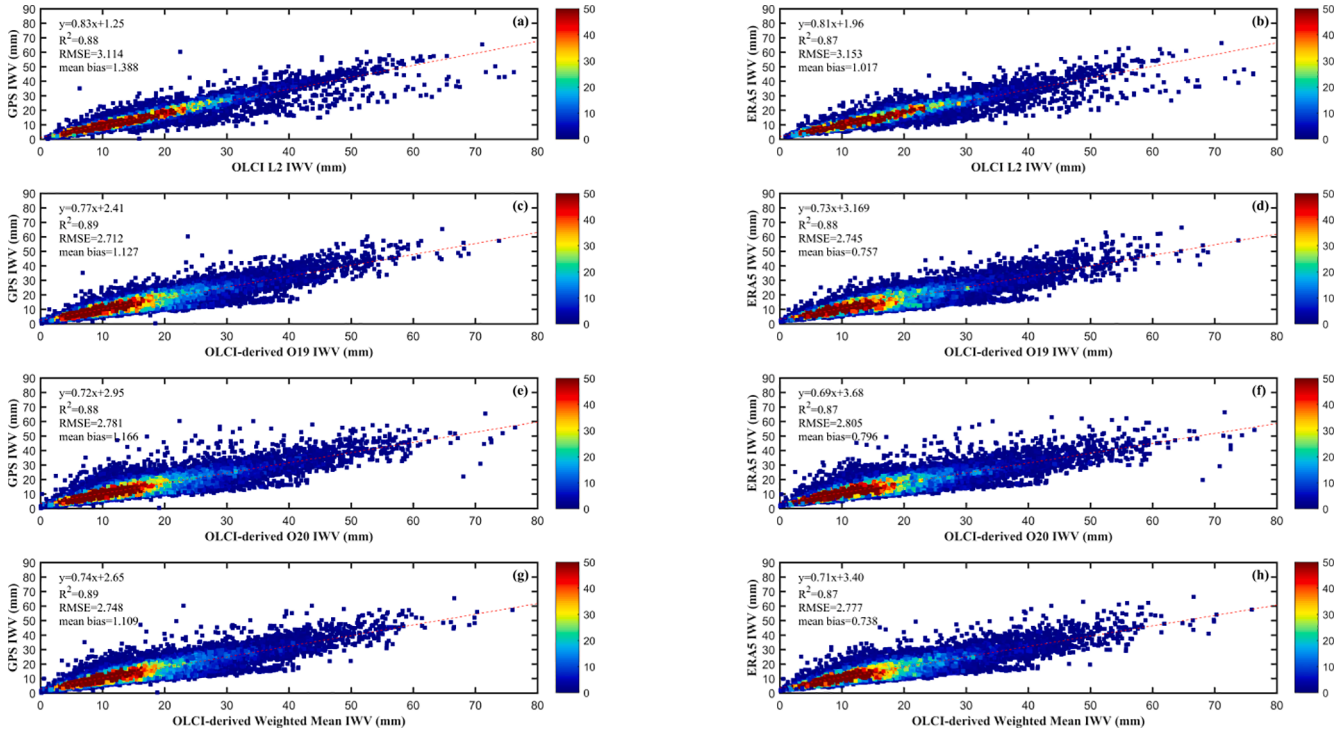

Fig. 4. Scatter-plots of the ground-based GPS-retrieved IWV versus (a) operational Level-2 OLCI IWV products, (c) IWV calculated using the new algorithm from OLCI band O19, (e) IWV calculated using the new algorithm from OLCI band O20, and (g) weighted mean IWV calculated using the new algorithm from OLCI bands O19 and O20. And the comparison of ECMWF ERA5 reanalysis IWV products with (b) operational Level-2 OLCI IWV products, (d) IWV calculated using the new algorithm from OLCI band O19, (f) IWV calculated using the new algorithm from OLCI band O20, and (h) weighted mean IWV calculated using the new algorithm from OLCI bands O19 and O20. The dashed red lines show the linear regression results of these data. The points colored with a rainbow scale illustrate the frequency of the water vapor values (brown most frequent, blue least frequent). (For interpretation of the references to color in this figure legend, the reader is referred to the web version of this article.)

showed a higher accuracy in spring and winter, and lower in summer and autumn, in terms of RMSE reduction compared to the operational OLCI L2 IWV data. The discrepancy was due to variation of atmospheric water vapor in different seasons. When atmospheric condition changes, the accuracies of water vapor retrieval from GPS and OLCI vary. Therefore, the performance of the retrieval algorithm is different.

4.4. *Land-surface-type analysis*

To investigate the quality of the new retrieved OLCI IWV data on different land surface types, we also selected four GPS stations representative of different land surface types, namely, Alice Springs (ALIC) station in a hot desert region, Blackville (BLCK) station in a temperate-climate vegetation region, Darwin (DARW) station in a tropical vegetation region, and Walgett (WLGT) station in an urban region (see Fig. 1). We selected these GPS stations since they had a relatively long observation period of IWV data, and they were situated in the different classical land-surface-type. The detailed information of these GPS sites is displayed in Table 6.

The overall validation results between new OLCI IWV data and the reference GPS-retrieved and ERA5 IWV data are illustrated in Fig. 7. In terms of RMSE reduction, the new retrieval method has a better accuracy compared to the Sentinel-3A IWV products, except for the new IWV estimated from OLCI O20 channel. In particular, the derived IWV from atmospheric water vapor O19 channel centered at 900 nm has the largest RMSE reduction, with a decrease of 11.28% from 3.465 mm to 3.074 mm when compared against the reference GPS IWV data; and 7.94% from 3.577 mm to 3.293 mm when compared against the reference ERA5 IWV data. For the weighted mean IWV estimations derived from the two absorption channels O19 and O20, the RMSE dropped from 3.465 mm to 3.374 mm when compared against the reference GPS IWV data; and from 3.577 mm to 3.565 mm compared to the reference ERA5 products. Nonetheless, there was a slight increase in RMSE values for the IWV retrieved from OLCI O20 channel when compared with the operational Level-2 OLCI IWV products. Its RMSE increased from 3.465 mm to 3.706 mm and from 3.577 mm to 3.884 mm when using GPS-sensed IWV and ERA5 IWV reference data, respectively. Overall, these OLCI IWV estimated from the new retrieval method had a good accuracy with an RMSE below 4 mm.

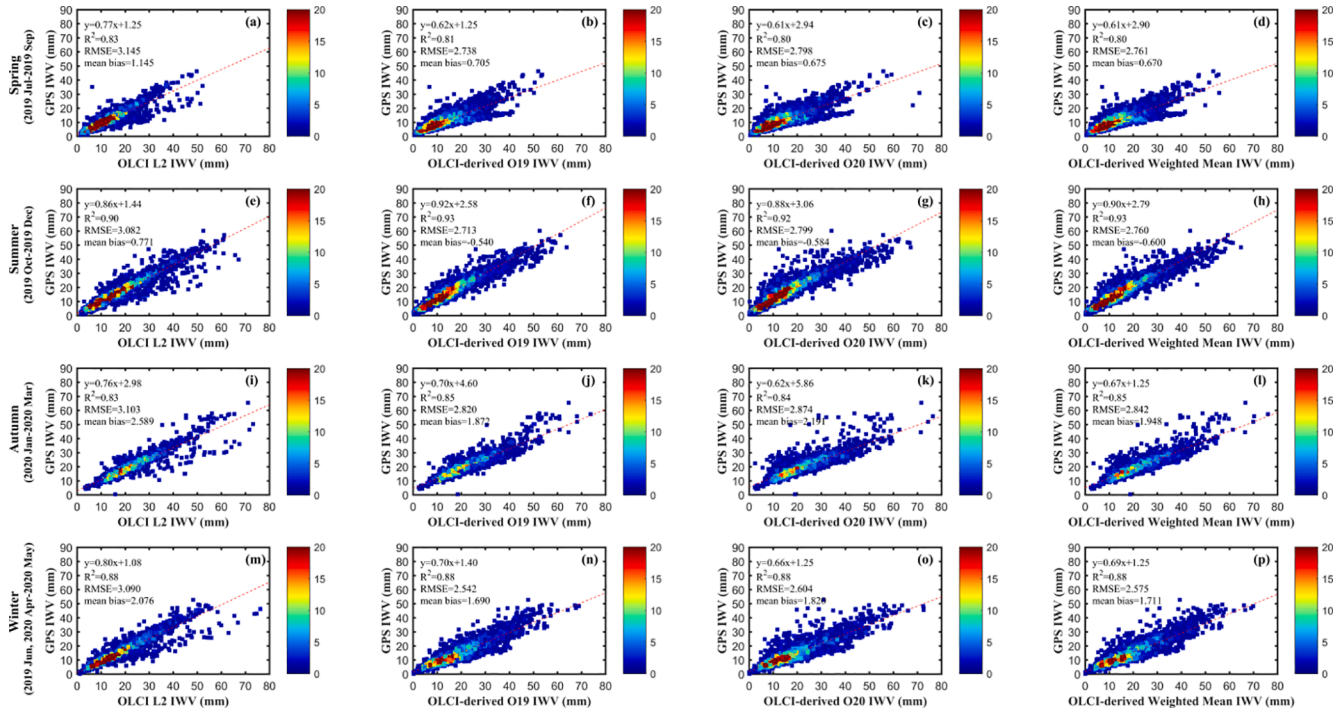

Fig. 5. Comparison of the in-situ GPS IWV with the operational Level-2 OLCI IWV products (first column), IWV calculated from new retrieval algorithm at OLCI channel O19 (second column), IWV calculated from new retrieval algorithm at OLCI channel O20 (third column), and weighted mean IWV calculated from new retrieval algorithm at OLCI channels O19 and O20 (last column), based on the season of spring, summer, autumn, and winter, respectively. The dashed red lines show the linear regression of these data. The points colored with a rainbow scale illustrate the frequency of the water vapor values (brown most frequent, blue least frequent). (For interpretation of the references to color in this figure legend, the reader is referred to the web version of this article.)

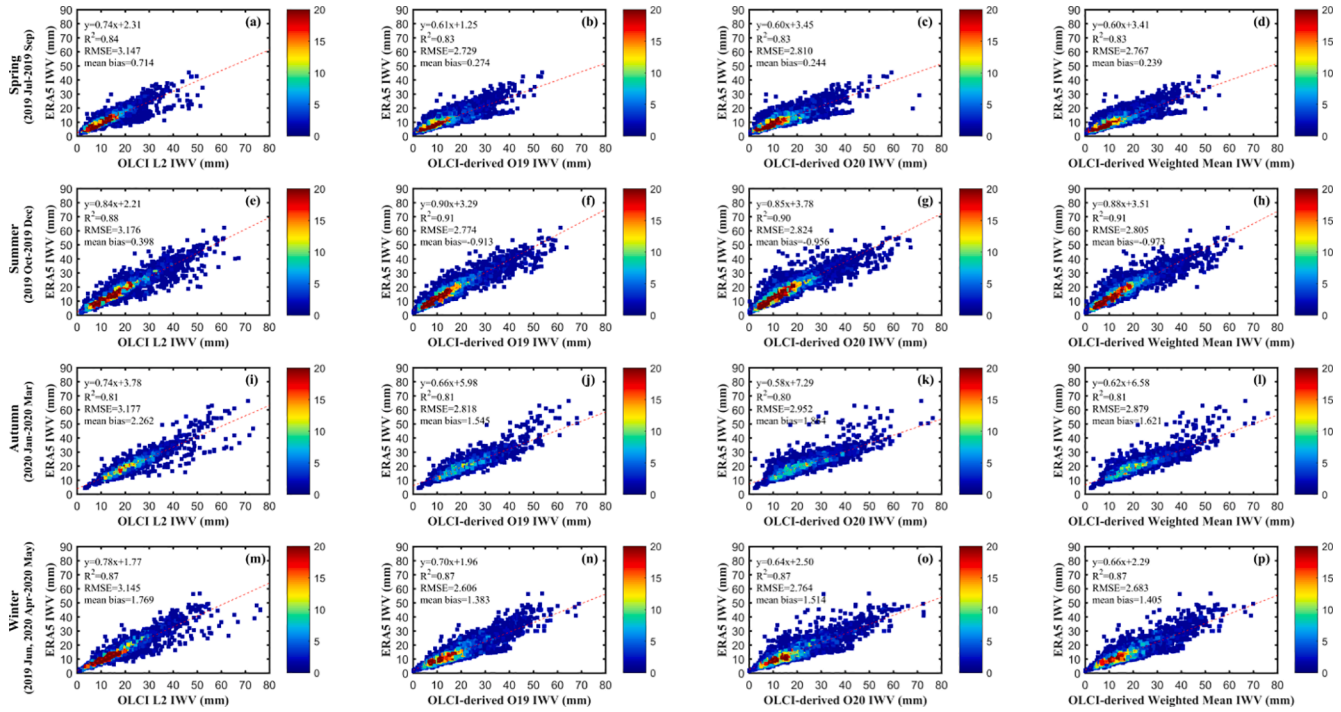

Fig. 6. Comparison of the ERA5 IWV with the operational Level-2 OLCI IWV products (first column), IWV calculated from new retrieval algorithm at OLCI channel O19 (second column), IWV calculated from new retrieval algorithm at OLCI channel O20 (third column), and weighted mean IWV calculated from new retrieval algorithm at OLCI channels O19 and O20 (last column), based on the season of spring, summer, autumn, and winter, respectively. The dashed red lines show the linear regression of these data. The points colored with a rainbow scale illustrate the frequency of the water vapor values (brown most frequent, blue least frequent). (For interpretation of the references to color in this figure legend, the reader is referred to the web version of this article.)

Table 5
Summary of RMSE (mm) and RMSE reductions (%) of the OLCI-derived IWV in comparison with the operational OLCI IWV products in each season.

			Sentinel-3A OLCI IWV product	New O19 IWV	New O20 IWV	New weighted mean IWV
Spring	GPS	RMSE	3.145	2.738	2.798	2.761
		RMSE reduction	–	12.94	11.03	12.21
	ERA5	RMSE	3.147	2.729	2.810	2.767
		RMSE reduction	–	13.28	10.71	12.07
Summer	GPS	RMSE	3.082	2.713	2.799	2.760
		RMSE reduction	–	11.97	9.18	10.45
	ERA5	RMSE	3.176	2.774	2.824	2.805
		RMSE reduction	–	12.66	11.08	11.68
Autumn	GPS	RMSE	3.103	2.820	2.874	2.842
		RMSE reduction	–	9.12	7.38	8.41
	ERA5	RMSE	3.177	2.818	2.952	2.879
		RMSE reduction	–	11.30	7.08	9.38
Winter	GPS	RMSE	3.090	2.542	2.604	2.575
		RMSE reduction	–	17.73	15.73	16.67
	ERA5	RMSE	3.145	2.606	2.764	2.683
		RMSE reduction	–	17.14	12.11	14.69

4.5. Station-based and daily time-series analysis

To study the performance of the new OLCI IWV retrieval method at different spatial locations, we showed in Fig. 8 the station-based RMSE map in Australia. Among the 453 GPS stations located in Australia, only GPS stations with more than 10 collocated data points were utilized in this study. In most GPS stations, the RMSE between new OLCI IWV estimates and reference IWV estimates from GPS and ERA5 was generally lower than that of the original OLCI L2 IWV product. In particular, the RMSE for the official OLCI L2 IWV product was in the range of 2 mm to 5 mm at most GPS sites. For the new OLCI IWV estimation, the RMSE at most GPS stations was in the range of 1 mm to 3 mm. The results indicate that the novel empirical water vapor retrieval algorithm can enhance the IWV retrieval accuracy.

In addition, we showed in Fig. 9 the daily comparison result between OLCI IWV and GPS (ERA5) IWV from June 1, 2019 to May 31, 2020 in Australia. The daily averaged IWV data were computed from the matched data points on a daily basis. Only the days with more than 10 matched data points were used. The daily variation trend of the new OCLI IWV retrievals showed a better agreement with reference GPS or ERA5 daily mean IWV data. The RMSE and mean bias were smaller compared to those of the original OLCI L2 IWV product. The daily averaged IWV difference between OLCI and GPS (ERA5) was relatively larger when the IWV values are large (IWV more than 20 mm), which was consistent with the recent work conducted by Xu and Liu. (2021). The result implied that our novel empirical water vapor model can also reduce the daily temporal difference between OLCI IWV and GPS (ERA5) IWV.

5. Discussion

Satellite-sensed observations have been employed widely to derive IWV content, due to its advantages of providing water vapor measurements over a large spatial coverage with a reasonable accuracy. This work aims to improve the retrieval accuracy of the IWV estimation from NIR bands of the OLCI instrument using a newly developed empirical regression model. Sentinel-3A OLCI provides IWV product for absorption channel O19 only. Our new model shows two advantages: (1) improving the IWV retrieval accuracy at channel O19 (900 nm); (2) being able to estimate IWV at another absorption channel O20 (940 nm). This is the first time in the research community to use both O19 and O20 channels to estimate water vapor from Sentinel-3A OLCI.

In contrast to widely used traditional retrieval methods, this novel retrieval approach does not need an atmospheric radiative transfer model. In the model development, the ground-based water vapor data between June 1, 2016 and May 31, 2019 from 453 GPS stations in Australia were utilized. The in-situ GPS IWV data from June 1, 2019 to May 31, 2020 were employed as reference water vapor values to independently validate the performance of the new retrieval algorithm.

The algorithm can enhance the retrieval accuracy of the OLCI NIR IWV observations. For the original OLCI L2 IWV product, the RMSE was 3.114 mm with respect to GPS IWV and 3.154 mm with respect to ERA5 IWV. The result was consistent with the recent work by Xu and Liu (2021). With the employment of the new empirical water vapor retrieval approach, the RMSE has reduced by 12.91% to 2.712 mm at the O19 channel, by 10.69% to 2.781 mm at the O20 channel, and by 11.75% to 2.748 mm for the weighted mean IWV when taking GPS IWV as reference. When taking ERA5 IWV as reference, it was respectively reduced by 12.94% to 2.745 mm, by 11.04% to 2.805 mm, and by 11.93% to 2.777 mm. The mean bias for all the new OLCI IWV estimates was in the range 1.109 mm to 1.166 mm compared with GPS IWV data, and in the range of 0.738 mm to 0.796 mm compared with ERA5 IWV data, all of which were lower than the official OLCI L2 IWV product (mean bias = 1.388 mm and 1.017 mm). Both original and new OLCI IWV observations tended to overestimate the IWV values with positive mean bias values.

In addition, the impacts of seasonal variation and land surface types on the performance of the new OLCI IWV retrieval model were also studied. Seasonal analysis results showed that the new OLCI IWV retrievals had a better seasonal agreement with the reference IWV data from GPS and ERA5 compared to the operational OLCI L2 IWV product. The seasonal reduction in RMSE was 11.03–12.94% in spring, 9.18–11.97% in summer, 7.38–9.12% in autumn, and 15.73–17.73% in winter when compared with reference GPS-measured IWV data. When compared with reference ERA5 IWV data, the seasonal RMSE reduction was 10.71–13.28%, 11.08–12.66%, 7.08–11.30%, and 12.11–17.14%, respectively. In terms of RMSE reduction, the reduction in spring and winter (dry seasons) was larger than that in summer and autumn (wet seasons). As for the different land-surface-type, the IWV accuracy at channel O19 using the new retrieval model was improved over the operational OLCI IWV products. However, the IWV estimated from the OLCI O20 channel using the new algorithm had a slightly lower accuracy.

The RMSE of the original OLCI L2 IWV products was in the range of 2

Table 6
Summary of data characteristics of in-situ GPS sites utilized for model verification.

Station	Longitude	Latitude	Height	Location	Characteristics	Observation period	Data pairs
ALIC	133.886	−23.670	603.278	Alice Springs	hot desert	June 2019 to May 2020	85
BLCK	150.245	−31.654	419.792	Blackville	vegetation areas		75
DARW	131.133	−12.844	125.143	Darwin	vegetation areas		73
WLGT	148.117	−30.023	170.231	Walgett	urban areas		99

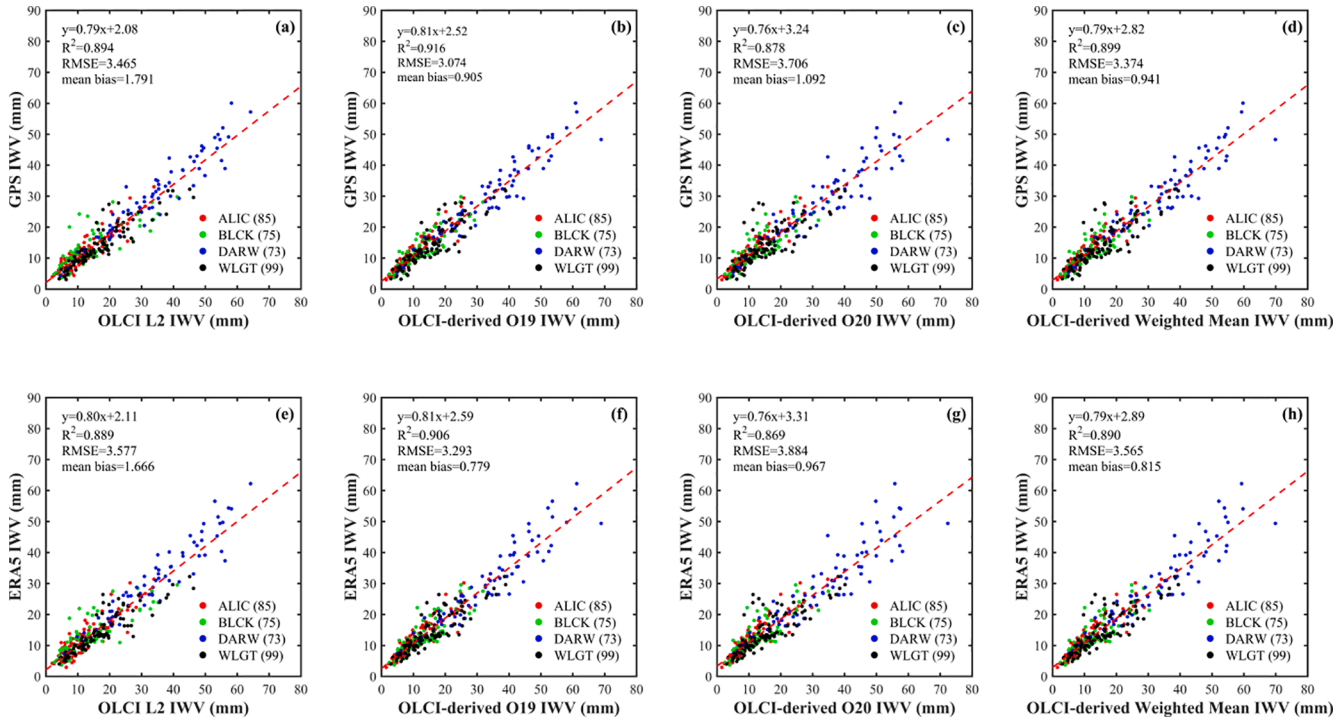

Fig. 7. Scatter plots of the ground-based GPS IWV against (a) the operational Level-2 OLCI IWV products, (b) IWV estimated from new retrieval algorithm at OLCI channel O19, (c) IWV estimated from new retrieval algorithm at OLCI channel O20, and (d) weighted mean IWV estimated from new retrieval algorithm at OLCI channels O19 and O20, and the ERA5 reanalysis IWV products against (e) the operational Level-2 OLCI IWV products, (f) IWV estimated from new retrieval algorithm at OLCI channel O19, (g) IWV estimated from new retrieval algorithm at OLCI channel O20, and (h) weighted mean IWV estimated from new retrieval algorithm at OLCI channels O19 and O20, at the locations of ALIC, BLCK, DARW, and WLGT GPS stations. The number in the parentheses after each GNSS station name is the number of data points at each station. The dashed red lines show the linear regression of these data.

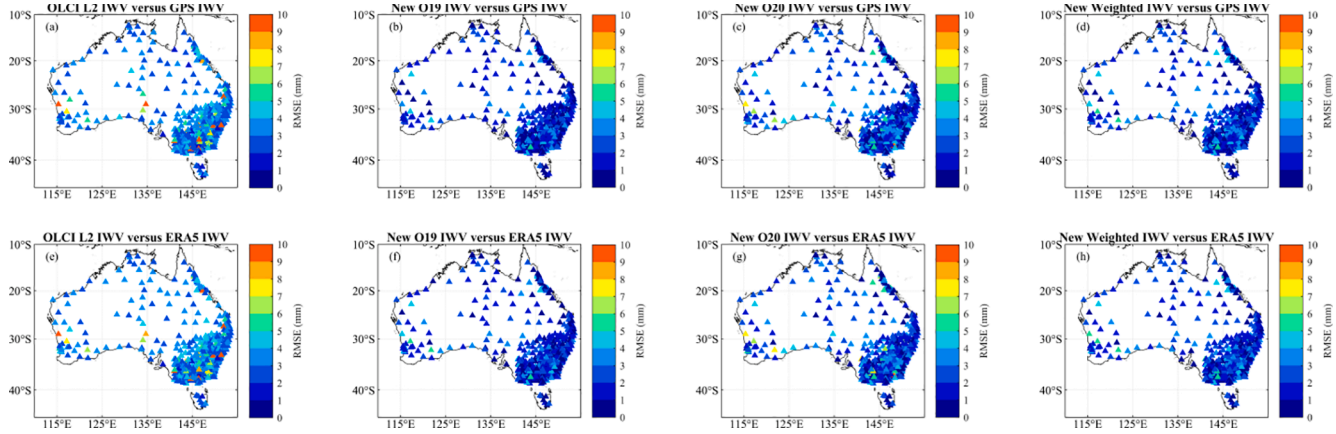

Fig. 8. Annual station-based RMSE between OLCI IWV measurements against both GPS-based and ERA5-based IWV measurements from June 1, 2019 to May 31, 2020 in Australia. (a)–(d): OLCI IWV versus GPS-based IWV at each ground-based GPS site. (e)–(h): OLCI IWV versus ERA5-based IWV at each ground-based GPS site.

mm to 5 mm at most GPS stations, while for all the new OLCI IWV retrievals the RMSE was in the range of 1 mm to 3 mm at most stations. It suggests that the algorithm could improve the spatial performance of IWV retrieval of OLCI IWV observations. As for the temporal performance, the daily variation trend of the new OCLI IWV data agreed better with that of reference GPS and ERA5, with lower RMSE and mean bias compared to the operational OLCI L2 IWV product. It suggests that the new OLCI IWV data showed better temporal performance over the operational OLCI L2 IWV product.

In general, the new empirical regression approach can improve the retrieval accuracy of OLCI NIR IWV measurements, with a smaller RMSE value than that of the OLCI official level-2 IWV products.

6. Conclusion

In this paper, we have developed a novel empirical regression model for OLCI NIR IWV retrieval with an improved retrieval accuracy. The performance of the model was independently evaluated using one year (June 1, 2019 to May 31, 2020) reference IWV data from both GPS and ERA5. The major findings from this work are summarized as follows.

(1) The new OLCI IWV data perform better with reference IWV data than the original OLCI L2 IWV product. The RMSE is reduced by 10.69–12.91% for GPS reference IWV data and by 11.04–12.94% for ERA5 reference IWV data;

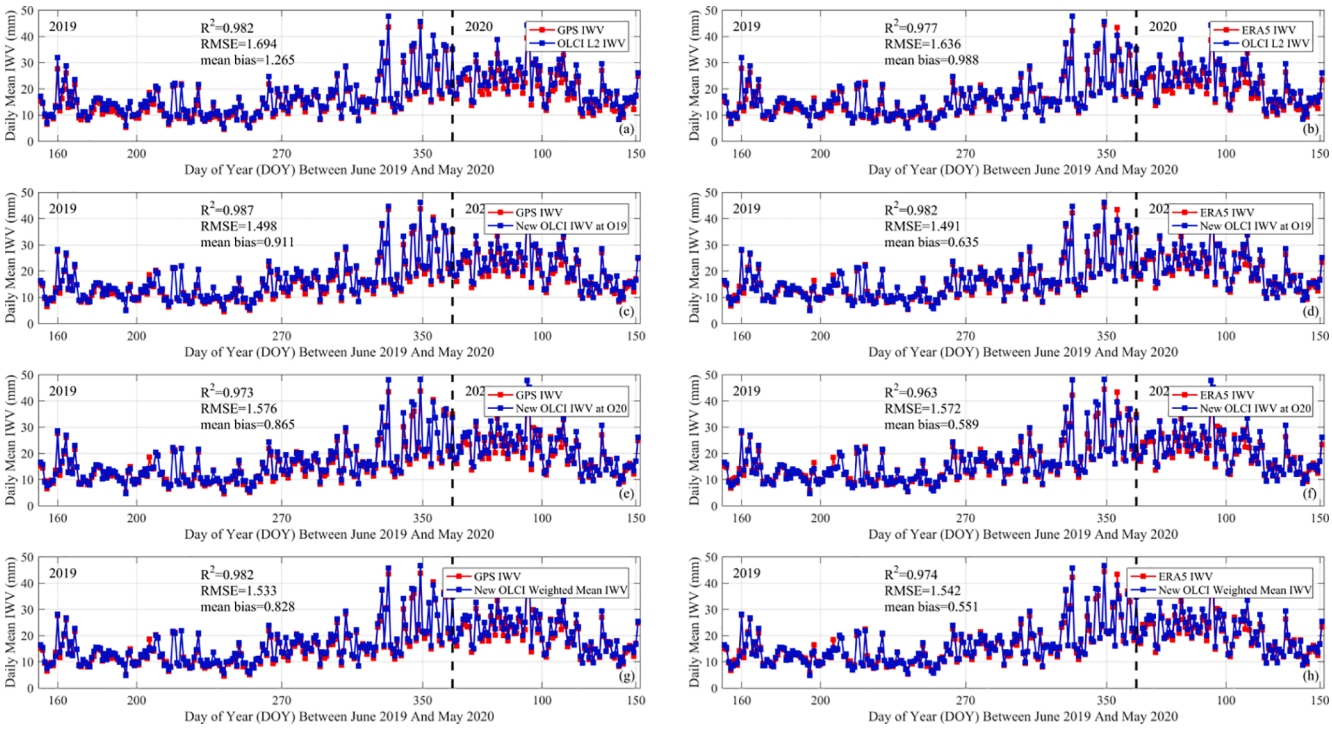

Fig. 9. Daily comparison time-series between the daily averaged IWV data from OLCI and GPS (ERA5) from June 1, 2019 to May 31, 2020 in Australia. (a) and (b) are the daily comparison of the original OLCI IWV product at channel O19 with respect to GPS IWV and ERA IWV, respectively; (c) and (d) are the daily comparison of the new OLCI IWV data at channel O19 with respect to GPS IWV and ERA IWV, respectively; (e) and (f) are the daily comparison of the new OLCI IWV data at channel O20 with respect to GPS IWV and ERA IWV, respectively; (g) and (h) are the daily comparison of the new OLCI weighted mean IWV data from both channels O19 and O20 with respect to GPS IWV and ERA IWV, respectively.

(2) Seasonal analysis showed that accuracy is high in dry seasons (spring and winter), but lower in wet seasons (summer and autumn). The new algorithm can improve the retrieval performance of the IWV estimation;
(3) Analysis of different land-surface types showed that the new OLCI IWV estimation had a better retrieval accuracy with reference IWV estimation than the operational OLCI L2 IWV product. However the accuracy of new OLCI IWV data from the O20 channel at 940 nm was slightly lower than the operational OLCI L2 IWV product;
(4) The difference between OLCI IWV against GPS and ERA5 IWV was reduced in both station-based and daily mean comparison after applying the new empirical water vapor retrieval method.

Overall, the developed regression retrieval approach can enhance the retrieval accuracy of the OLCI NIR band at O19. The enhanced IWV data could play a more important role in weather forecasting, climate monitoring, and many other applications.

Declaration of Competing Interest

The authors declare that they have no known competing financial interests or personal relationships that could have appeared to influence the work reported in this paper.

Acknowledgment

This work was supported in part by the Key Program of the National Natural Science Foundation of China under Project 41730109, in part by the Hong Kong Research Grants Council (RGC) under Project Q73B PolyU 15211919, and in part by the Emerging Frontier Area (EFA) Scheme of The Research Institute for Sustainable Urban Development is under the Hong Kong Polytechnic University, Hong Kong, China. (RISUD) of The Hong Kong Polytechnic University under Grant 1-BBWJ. The authors would like to thank the JAG editorial team and the three anonymous reviewers for their valuable comments that help improve the quality of this manuscript. The authors are grateful for Sentinel-3 OLCI data provided by the European Space Agency (ESA). The authors also gratefully acknowledge the support by the Geoscience Australia for sharing the GPS tropospheric products. The European Centre for Medium-Range Weather Forecasts (ECMWF) is acknowledged for providing the reanalysis water vapor data.

References

Abbasi, B., Qin, Z., Du, W., Fan, J., Zhao, C., Hang, Q., Zhao, S., Li, S., 2020. An algorithm to retrieve total precipitable water vapor in the atmosphere from FengYun 3D medium resolution spectral imager 2 (FY-3D MERSI-2) data. Remote Sens. 12, 3469. https://doi.org/10.3390/rs12213469.

Bennartz, R., Fischer, J., 2001. Retrieval of columnar water vapour over land from backscattered solar radiation using the Medium Resolution Imaging Spectrometer. Remote Sens. Environ. 78, 274–283.

Bevis, M., Businger, S., Herring, T.A., Rocken, C., Anthes, R.A., Ware, R.H., 1992. GPS meteorology: remote sensing of atmospheric water vapor using the global positioning system. J. Geophys. Res. Atmospheres 97, 15787–15801. https://doi.org/10.1029/92JD01517.

Bojinski, S., Verstraete, M., Peterson, T.C., Richter, C., Simmons, A., Zemp, M., 2014. The concept of essential climate variables in support of climate research, applications, and policy. Bull. Am. Meteorol. Soc. 95, 1431–1443.

Chen, B., Liu, Z., 2015. A comprehensive evaluation and analysis of the performance of multiple tropospheric models in China region. IEEE Trans. Geosci. Remote Sens. 54, 663–678.

Colman, R., 2003. A comparison of climate feedbacks in general circulation models. Clim. Dyn. 20, 865–873. https://doi.org/10.1007/s00382-003-0310-z.

Davies, O.T., Watson, P.A., 1998. Comparison of integrated precipitable water vapour obtained by GPS and radiosondes. Electron. Lett. 34, 645–646. https://doi.org/10.1049/el:19980633.

Donlon, C., Berruti, B., Buongiorno, A., Ferreira, M.-H., Féménias, P., Frerick, J., Goryl, P., Klein, U., Laur, H., Mavrocordatos, C., Nieke, J., Rebhan, H., Seitz, B., Stroede, J., Sciarra, R., 2012. The global monitoring for environment and security (GMES) Sentinel-3 mission. Remote Sens. Environ. Sentinel Miss. – New Opport. Sci. 120, 37–57. https://doi.org/10.1016/j.rse.2011.07.024.

Ebita, A., Kobayashi, S., Ota, Y., Moriya, M., Kumabe, R., Onogi, K., Harada, Y., Yasui, S., Miyaoka, K., Takahashi, K., Kamahori, H., Kobayashi, C., Endo, H., Soma, M., Oikawa, Y., Ishimizu, T., 2011. The Japanese 55-year reanalysis "JRA-55": an interim report. Sola 7, 149–152. https://doi.org/10.2151/sola.2011-038.

Fischer, J., Leinweber, R., and Preusker, R., 2010a. Retrieval of Total Water Vapor Content from OLCI Measurements. Available: https://sentinels.copernicus.eu/documents/247904/349589/OLCI_L2_ATBD_Water_Vapour.pdf/228fcc63-7e26-4dfa-b541-deba67feb62f?t=1371548280000.

Fischer, J., Leinweber, R., and Preusker, R., 2010b. Retrieval of Total Water Vapor Content from MERIS Measurements. Available: https://earth.esa.int/documents/700255/2042855/MERIS_ATBD_2.4_v4.2+-+2011.pdf.

Fletcher, K., 2010. Sentinel-3: ESA's Global Land and Ocean Mission for GMES Operational Services. Available: https://sentinel.esa.int/documents/247904/351187/S3_SP-1322_3.pdf.

Fragkos, K., Antonescu, B., Giles, D.M., Ene, D., Boldeanu, M., Efstathiou, G.A., Belegante, L., Nicolae, D., 2019. Assessment of the total precipitable water from a sun photometer, microwave radiometer and radiosondes at a continental site in southeastern Europe. Atmospheric Meas. Tech. 12, 1979–1997. https://doi.org/10.5194/amt-12-1979-2019.

Gao, B.-C., Goetz, A.F., 1990. Column atmospheric water vapor and vegetation liquid water retrievals from airborne imaging spectrometer data. J. Geophys. Res. Atmospheres 95, 3549–3564.

Gao, B.-C., Kaufman, Y.J., 2003. Water vapor retrievals using Moderate Resolution Imaging Spectroradiometer (MODIS) near-infrared channels. J. Geophys. Res. Atmospheres 108. https://doi.org/10.1029/2002JD003023.

Gong, S., Chen, W., Zhang, C., Wu, P., Han, J., 2020. Intercomparisons of precipitable water vapour derived from radiosonde, GPS and sunphotometer observations. Geod. Vestn. 64, 562–577. https://doi.org/10.15292/geodetski-vestnik.2020.04.562-577.

Gong, S., Fiifi Hagan, D., Lu, J., Wang, G., 2018a. Validation on MERSI/FY-3A precipitable water vapor product. Adv. Space Res. 61, 413–425. https://doi.org/10.1016/j.asr.2017.10.005.

Gong, S., Hagan, D.F.T., Wu, X., Wang, G., 2018b. Spatio-temporal analysis of precipitable water vapour over northwest china utilizing MERSI/FY-3A products. Int. J. Remote Sens. 39, 3094–3110. https://doi.org/10.1080/01431161.2018.1437298.

He, J., Liu, Z., 2019. Comparison of satellite-derived precipitable water vapor through near-infrared remote sensing channels. IEEE Trans. Geosci. Remote Sens. 57, 10252–10262.

Held, I.M., Soden, B.J., 2000. Water vapor feedback and global warming. Annu. Rev. Energy Environ. 25, 441–475.

Hersbach, H., Bell, B., Berrisford, P., Hirahara, S., Horanyi, A., Munoz-Sabater, J., Nicolas, J., Peubey, C., Radu, R., Schepers, D., Simmons, A., Soci, C., Abdalla, S., Abellan, X., Balsamo, G., Bechtold, P., Biavati, G., Bidlot, J., Bonavita, M., De Chiara, G., Dahlgren, P., Dee, D., Diamantakis, M., Dragani, R., Flemming, J., Forbes, R., Fuentes, M., Geer, A., Haimberger, L., Healy, S., Hogan, R.J., Holm, E., Janiskova, M., Keeley, S., Laloyaux, P., Lopez, P., Lupu, C., Radnoti, G., de Rosnay, P., Rozum, I., Vamborg, F., Villaume, S., Thepaut, J.-N., 2020. The ERA5 global reanalysis. Q. J. R. Meteorol. Soc. 146, 1999–2049. https://doi.org/10.1002/qj.3803.

Hoffmann, L., Günther, G., Li, D., Stein, O., Wu, X., Griessbach, S., Heng, Y., Konopka, P., Müller, R., Vogel, B., Wright, J., 2019. From ERA-Interim to ERA5: The considerable impact of ECMWF's next-generation reanalysis on Lagrangian transport simulations. Atmospheric Chem. Phys. 19, 3097–3124. https://doi.org/10.5194/acp-19-3097-2019.

Holben, B.N., Eck, T.F., Slutsker, I. al, Tanre, D., Buis, J.P., Setzer, A., Vermote, E., Reagan, J.A., Kaufman, Y.J., Nakajima, T., 1998. AERONET—A federated instrument network and data archive for aerosol characterization. Remote Sens. Environ. 66, 1–16.

Kalnay, E., Kanamitsu, M., Kistler, R., Collins, W., Deaven, D., Gandin, L., Iredell, M., Saha, S., White, G., Woollen, J., Zhu, Y., Chelliah, M., Ebisuzaki, W., Higgins, W., Janowiak, J., Mo, K.C., Ropelewski, C., Wang, J., Leetmaa, A., Reynolds, R., Jenne, R., Joseph, D., 1996. The NCEP/NCAR 40-year reanalysis project. Bull. Am. Meteorol. Soc. 77, 437–471. https://doi.org/10.1175/1520-0477(1996)077<0437:TNYRP>2.0.CO;2.

Kaufman, Y.J., Gao, B.-C., 1992. Remote sensing of water vapor in the near IR from EOS/MODIS. IEEE Trans. Geosci. Remote Sens. 30, 871–884.

King, M.D., Menzel, W.P., Kaufman, Y.J., Tanré, D., Gao, B.-C., Platnick, S., Ackerman, S. A., Remer, L.A., Pincus, R., Hubanks, P.A., 2003. Cloud and aerosol properties, precipitable water, and profiles of temperature and water vapor from MODIS. IEEE Trans. Geosci. Remote Sens. 41, 442–458.

Lamquin, N., Clerc, S., Bourg, L., Donlon, C., 2020. OLCI A/B Tandem Phase Analysis, Part 1: Level 1 Homogenisation and Harmonisation. Remote Sens. 12, 1804. https://doi.org/10.3390/rs12111804.

Lang, R., Williams, J.E., Van Der Zande, W.J., Maurellis, A.N., 2003. Application of the Spectral Structure Parameterization technique: retrieval of total water vapor columns from GOME.

Liu, H., Li, H., Tang, S., Duan, M., Zhang, S., Deng, X., Hu, J., 2020. A physical algorithm for precipitable water vapour retrieval over land using passive microwave observations. Int. J. Remote Sens. 41, 6288–6306. https://doi.org/10.1080/01431161.2020.1737337.

Mertikas, S., Partsinevelos, P., Tripolitsiotis, A., Kokolakis, C., Petrakis, G., Frantzis, X., 2020. Validation of sentinel-3 OLCI integrated water vapor products using regional GNSS measurements in Crete, Greece. Remote Sens. 12, 2606. https://doi.org/10.3390/rs12162606.

Ning, T., Wang, J., Elgered, G., Dick, G., Wickert, J., Bradke, M., Sommer, M., Querel, R., Smale, D., 2016. The uncertainty of the atmospheric integrated water vapour estimated from GNSS observations. Atmospheric Meas. Tech. 9, 79–92. https://doi.org/10.5194/amt-9-79-2016.

Pigram, C., 2012. Geoscience Australia – a multi disciplined agency. Episodes J. Int. Geosci. 35, 524–525. https://doi.org/10.18814/epiiugs/2012/v35i4/009.

Schläpfer, D., Borel, C.C., Keller, J., Itten, K.I., 1998. Atmospheric precorrected differential absorption technique to retrieve columnar water vapor. Remote Sens. Environ. 65, 353–366. https://doi.org/10.1016/S0034-4257(98)00044-3.

Seemann, S.W., Li, J., Menzel, W.P., Gumley, L.E., 2003. Operational retrieval of atmospheric temperature, moisture, and ozone from MODIS infrared radiances. J. Appl. Meteorol. Climatol. 42, 1072–1091. https://doi.org/10.1175/1520-0450(2003)042<1072:OROATM>2.0.CO;2.

Sobrino, J.A., Jimenez-Munoz, J.C., Mattar, C., Soria, G., 2015. Evaluation of Terra/MODIS atmospheric profiles product (MOD07) over the Iberian Peninsula: a comparison with radiosonde stations. Int. J. Digit. Earth 8, 771–783. https://doi.org/10.1080/17538947.2014.936973.

Su, Z., Fernández-Prieto, D., Timmermans, J., Chen, X., Hungershoefer, K., Roebeling, R., Schröder, M., Schulz, J., Stammes, P., Wang, P., Wolters, E., 2014. First results of the earth observation Water Cycle Multi-mission Observation Strategy (WACMOS). Int. J. Appl. Earth Obs. Geoinformation 26, 270–285. https://doi.org/10.1016/j.jag.2013.08.002.

Trenberth, K.E., Fasullo, J., Smith, L., 2005. Trends and variability in column-integrated atmospheric water vapor. Clim. Dyn. 24, 741–758.

Turner, D.D., Clough, S.A., Liljegren, J.C., Clothiaux, E.E., Cady-Pereira, K.E., Gaustad, K. L., 2007. Retrieving liquid water path and precipitable water vapor from the atmospheric radiation measurement (ARM) microwave radiometers. IEEE Trans. Geosci. Remote Sens. 45, 3680–3690.

Vaquero-Martínez, J., Antón, M., de Galisteo, J.P.O., Cachorro, V.E., Álvarez-Zapatero, P., Román, R., Loyola, D., Costa, M.J., Wang, H., Abad, G.G., 2018. Inter-comparison of integrated water vapor from satellite instruments using reference GPS data at the Iberian Peninsula. Remote Sens. Environ. 204, 729–740.

Vaquero-Martínez, J., Antón, M., de Galisteo, J.P.O., Cachorro, V.E., Costa, M.J., Román, R., Bennouna, Y.S., 2017. Validation of MODIS integrated water vapor product against reference GPS data at the Iberian Peninsula. Int. J. Appl. Earth Obs. Geoinformation 63, 214–221.

Wang, H., Liu, X., Chance, K., González Abad, G., Chan Miller, C., 2014. Water vapor retrieval from OMI visible spectra. Atmospheric Meas. Tech. 7, 1901–1913.

Wang, S., Xu, T., Nie, W., Jiang, C., Yang, Y., Fang, Z., Li, M., Zhang, Z., 2020. Evaluation of precipitable water vapor from five reanalysis products with ground-based GNSS observations. Remote Sens. 12, 1817. https://doi.org/10.3390/rs12111817.

Wang, X., Zhang, K., Wu, S., Fan, S., Cheng, Y., 2016. Water vapor-weighted mean temperature and its impact on the determination of precipitable water vapor and its linear trend. J. Geophys. Res. Atmospheres 121, 833–852. https://doi.org/10.1002/2015JD024181.

Xu, J., Liu, Z., 2021. The first validation of sentinel-3 OLCI integrated water vapor products using reference GPS data in Mainland China. IEEE Trans. Geosci. Remote Sens. 1–17 https://doi.org/10.1109/TGRS.2021.3099168.

Yu, C., Li, Z., Blewitt, G., 2021. Global comparisons of ERA5 and the operational HRES tropospheric delay and water vapor products with GPS and MODIS. e2020EA001417 Earth Space Sci. 8. https://doi.org/10.1029/2020EA001417.